The Journal of Chemical Physics

RESEARCH ARTICLE | JUNE 15 2023

Ice breakloose friction

Special Collection: Adhesion and Friction

B. N. J. Persson ; E. C. Tyrode

J. Chem. Phys. 158, 234701 (2023)
https://doi.org/10.1063/5.0155545

The Journal of Chemical Physics ARTICLE scitation.org/journal/jcp

Ice breakloose friction

Cite as: J. Chem. Phys. 158, 234701 (2023); doi: 10.1063/5.0155545
Submitted: 21 April 2023 • Accepted: 25 May 2023 •
Published Online: 15 June 2023

B. N. J. Persson[1,2,a)] and E. C. Tyrode[3]

AFFILIATIONS

[1] Peter Grünberg Institute (PGI-1), Forschungszentrum Jülich, 52425 Jülich, Germany
[2] MultiscaleConsulting, Wolfshovener Str. 2, 52428 Jülich, Germany
[3] Department of Chemistry, School of Engineering Sciences in Chemistry, Biotechnology and Health, KTH Royal Institute of Technology, SE-114 28 Stockholm, Sweden

Note: This paper is part of the JCP Special Topic on Adhesion and Friction.
[a)] **Author to whom correspondence should be addressed:** b.persson@fz-juelich.de

ABSTRACT

We discuss the origin of the breakloose (or static) friction force when an ice block is slid on a hard randomly rough substrate surface. If the substrate has roughness with small enough amplitude (of order a 1 nm or less), the breakloose force may be due to interfacial slip and is determined by the elastic energy per unit area, U_{el}/A_0, stored at the interface after the block has been displaced a short distance from its original position. The theory assumes complete contact between the solids at the interface and that there is no elastic deformation energy at the interface in the original state before the application of the tangential force. The breakloose force depends on the surface roughness power spectrum of the substrate and is found to be in good agreement with experimental observations. We show that as the temperature decreases, there is a transition from interfacial sliding (mode II crack propagation, where the crack propagation energy $G_{II} = U_{el}/A_0$) to opening crack propagation (mode I crack propagation with G_I the energy per unit area to break the ice–substrate bonds in the normal direction).

I. INTRODUCTION

Friction on ice is a fascinating topic with a long history.[1–22] Pioneering work was done by Faraday more than 150 years ago.[23] He proposed that the surface of ice is covered by a liquid-like water layer, now understood as a result of premelting, which is a very common phenomenon for crystalline solids.[24–33] Thomson suggested instead that the liquid-like layer was due to pressure melting, as observed for materials that at the melting temperature have a bigger volume in the solid state than in the fluid state.[34] Pressure melting was often used as an explanation for the low friction on ice for the following 80 years or so, until Bowden and Hughes suggested that frictional heating might result in melting of the ice surface and that this was the main reason for the low friction of ice at high enough sliding speeds.[35] Yet, frictional heating cannot explain why the surface of ice remains slippery when standing still or at low sliding speeds. These observations were resolved by reconsidering Faraday's original premolten layer proposal and confirming its existence using a battery of modern experimental techniques.[1,30,31] Why does ice exhibit a nonzero friction force as the sliding speed $v \to 0$ if a liquid-like premelted water film separates the surfaces at the sliding interface? For an elastically hard solid with large surface roughness, a contribution to the friction force on ice comes from plowing of the ice by the hard asperities of the counter (substrate) surface. However, for a perfectly smooth substrate surface, one would expect a much smaller friction coefficient than observed when the solids are separated by a premelted water film with water-like viscosity. Shearing of a water film with the thickness $d = 1$ nm results in a viscous frictional shear stress $\tau = \eta v/d \approx 1$ kPa when the sliding speed is $v = 1$ mm s^{-1}. If the ice has large enough surface roughness, the contact pressure in the ice contact regions will be of the same order as the ice penetration hardness, which is typically $\sigma_P \approx 10$ MPa, giving the friction coefficient $\mu = \eta v/(\sigma_P d) \approx 10^{-4}$, which is much smaller than usually observed for the sliding speed $v = 1$ mm s^{-1}. In reality, the premelted water film may have larger effective viscosity than water and may exhibit shear thinning,[50] but one would still expect $\mu \to 0$ as $v \to 0$, which is not observed.

Experiments have shown that there is a premelted water film at the interface between (hydrophilic) silica glass and ice.[36–38] When a

tangential force displaces an ice block frozen on a silica surface, it is usually found that the slip plane is located not at the ice–silica interface but in the ice (cohesive failure). However, for very smooth silica surfaces, the slip occurs at the ice–silica interface (adhesive failure). Thus, for a silica surface with the root-mean-square (rms) roughness $h_{\rm rms} \approx 7.5$ nm, only cohesive failure was observed, while on a silica surface with $h_{\rm rms} \approx 0.45$ nm (when measured over a $2 \times 2\ \mu m^2$ surface area), interfacial sliding occurred for temperatures between 0 and $-20\,^\circ$C and cohesive failure for $T < -25\,^\circ$C (see Ref. 36). For $-25\,^\circ\text{C} < T < -20\,^\circ$C, adhesive failure (but no sliding) occurred, i.e., no ice could be detected remaining on the silica surface. When interfacial sliding takes place, the maximum (or breakloose) shear stress $\tau_{\rm max}$ increases linearly with the difference between the ice bulk melting temperature and the actual temperature, $T_{\rm m} - T$, with $\tau_{\rm max} \approx 0.75$ MPa at $T = -20\,^\circ$C. This result was tentatively explained by the assumption of a premelted liquid-like water film at the ice–silica interface for $T > -20\,^\circ$C, as verified in Ref. 36 using several other experimental methods.

Here, we will discuss the origin of the breakloose force for ice in contact with a hard randomly rough substrate surface. We will assume that the substrate surface is so smooth that (because of adhesion) the ice (with the premelted water film) is in complete contact with it at any stage in the sliding act. We also assume that in the initial state, there are no stress and elastic deformations in the ice induced by the roughness of the substrate surface. This is the case if the ice is formed by freezing water on the substrate surface or if the ice is pressed against the substrate and left for sufficiently long time that the stress field initially generated in the vicinity of the hard substrate asperities can relax by creep or regelation to a nearly stress free state. We assume that a thin liquid-like film occurs at the ice–silica interface (due to ice premelting) and that the (viscous) frictional shear stress can be neglected. We show that as the temperature decreases, there is a transition from interfacial sliding (mode II crack propagation, where the crack propagation energy $G_{\rm II} = U_{\rm el}/A_0$) to opening crack propagation (mode I crack propagation with $G_{\rm I}$ the energy per unit area to break the ice–substrate bonds in the normal direction).

II. THEORY

Consider applying a tangential force to an ice block in full contact with a hard randomly rough substrate. We assume first that the interface displaces uniformly laterally in response to the applied tangential force, but later we will show that the breakloose friction involves frictional (type II) crack propagation. We assume no pressure melting or plastic deformation of the ice and that no change occur in the ice surface topography due to flow of the premelted water film from high pressure to low pressure interfacial regions, where it could freeze (regelation resulting from premelting, see Fig. 5).

Under the assumptions above, it is easy to derive an expression for the breakloose force. Let $h(\mathbf{x})$ be the surface roughness profile of the substrate. When the bottom surface of the ice block has moved the lateral distance $\mathbf{s} = s\hat{x}$, the ice surface deforms elastically in response to the change in the surface roughness profile it experiences. The normal displacement field is

$$u(\mathbf{x}) = h(\mathbf{x}+\mathbf{s}) - h(\mathbf{x}).$$

We define

$$u(\mathbf{q}) = \frac{1}{(2\pi)^2}\int d^2x\ u(\mathbf{x})e^{-i\mathbf{q}\cdot\mathbf{x}}$$

so that

$$u(\mathbf{q}) = h(\mathbf{q})\left(e^{-i\mathbf{q}\cdot\mathbf{s}} - 1\right). \tag{1}$$

The elastic energy stored in the resulting deformation field is[39]

$$U_{\rm el} = (2\pi)^2\frac{E^*}{4}\int d^2q\ q\langle u(\mathbf{q})u(-\mathbf{q})\rangle, \tag{2}$$

where $\langle\cdots\rangle$ stands for ensemble averaging and where E^* is the effective Young's modulus, which for a rigid substrate is given by $E^* = E/(1-\nu^2)$, where E and ν are Young's modulus and Poisson's ratio of the ice. Using (1) and (2), we get

$$U_{\rm el} = (2\pi)^2\frac{E^*}{4}\int d^2q\ q\langle h(\mathbf{q})h(-\mathbf{q})\rangle 2[1-\cos(\mathbf{q}\cdot\mathbf{s})].$$

Since the surface roughness power spectrum is[39,40]

$$C(\mathbf{q}) = \frac{(2\pi)^2}{A_0}\langle h(\mathbf{q})h(-\mathbf{q})\rangle, \tag{3}$$

where A_0 is the surface area, we get

$$U_{\rm el} = \frac{1}{2}E^*A_0\int d^2q\ qC(\mathbf{q})[1-\cos(\mathbf{q}\cdot\mathbf{s})].$$

Using the integral representation of the Bessel function of order 0,

$$J_0(x) = \frac{1}{2\pi}\int_0^{2\pi} d\phi\ \cos(x\cos\phi),$$

and introducing polar coordinates in $\mathbf{q}$-space with $d^2q = dqqd\phi$, we get

$$U_{\rm el} = \pi E^*A_0\int_{q_0}^{q_1} dq\ q^2C(q)[1-J_0(qs)], \tag{4}$$

where we have assumed isotropic surface roughness so the power spectrum depends on only $|\mathbf{q}| = q$ and not the angle ϕ. The force $F = dU_{\rm el}/ds$ is given by

$$F = \pi E^*A_0\int_{q_0}^{q_1} dq\ q^3C(q)J_1(qs), \tag{5}$$

where $J_1(x) = -J_0'(x)$ is the Bessel function of order 1. Using that for small x, we have $J_1(x) \approx x/2$, and we get $F \approx ks$ as $s \to 0$, where

$$k = E^*A_0\frac{\pi}{2}\int_{q_0}^{q_1} dq\ q^4C(q).$$

Note that the mean square slope and the mean square curvature of the surface are determined by[41,42]

$$\xi^2 = 2\pi\int_{q_0}^{q_1} dq\ q^3C(q), \qquad \kappa^2 = \pi\int_{q_0}^{q_1} dq\ q^5C(q),$$

which both are usually determined mainly by the shortest wavelength surface roughness. This is, therefore, also the case for k and for the maximum $F_{\rm max}$ of the $F(s)$ curve.

It is clear from (5) that scaling the power spectrum with a factor g^2 will increase the breakloose force with the same factor g^2. Scaling $C(q)$ by g^2 is equivalent with scaling $h(\mathbf{x})$ with a factor of g. Thus, the breakloose force will scale with the rms surface roughness $h_{\rm rms}$ as $h_{\rm rms}^2$. For a self-affine fractal surface, it is also clear that increasing the fractal dimension $D_{\rm f}$ (which is equivalent to reducing the Hurst exponent H) but keeping the rms roughness amplitude and the roll-off wavenumber unchanged will increase the breakloose force as the short wavelength roughness is increased by this transformation. Similarly keeping $h_{\rm rms}$ and H constant but increasing the roll-off wavenumber of the power spectrum will increase the amplitude of the short wavelength roughness and, hence, the breakloose force. For self-affine fractal surfaces with the power spectrum

$$C(q) = C_0\left(\frac{q}{q_0}\right)^{-2(1+H)}$$

for $q_0 < q < q_1$ and zero otherwise, the asymptotic value for $U_{\rm el}/A_0$ for large displacement is given by (see Appendix A)

$$\frac{U_{\rm el}}{A_0} = \frac{E^*\xi^2}{q_0}\frac{1-H}{1-2H}\frac{1-(q_1/q_0)^{1-2H}}{1-(q_1/q_0)^{2-2H}}.$$

To study the dependency of F and $U_{\rm el}$ on the displacement s quantitatively, we have performed numerical calculations using a realistic surface roughness power spectrum.

III. SURFACE ROUGHNESS POWER SPECTRUM

We have measured the surface topography of flat fused silica widows obtained from Thorlabs (super polished mirror blank 2 Å), which is similar to the samples studied in Ref. 36 (which were obtained from Laser Components GmbH, Olching, Germany). The topography measurements were obtained using a MultiMode8 atomic force microscope (AFM, Bruker) operated in ScanAsyst imaging mode. The images were recorded with ScanAsyst-air cantilevers with a tip radius of 2 nm and a spring constant of 0.4 N/m. From the measured height profile $z = h(x, y)$, we have calculated the surface roughness power spectra using (3).

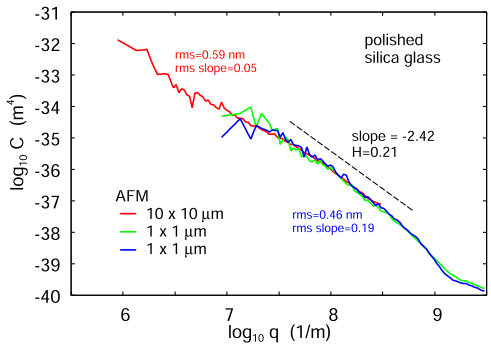

FIG. 1. The surface roughness power spectrum of the silica substrate as obtained from AFM topography measurements (1024 × 1024 data points) over square areas with the side 10 μm (red curve) and 1 μm (green and blue curves). The rms-roughness values are 0.59, 0.48, and 0.46 nm and the rms-slopes are 0.05, 0.20, and 0.19, for the red, green, and blue curves, respectively. The slope of the dashed line correspond to the Hurst exponent $H \approx 0.21$.

Figure 1 shows the surface roughness power spectrum of the silica surface as obtained from AFM topography measurements (1024 × 1024 data points) over square areas with the side 10 μm (red curve) and 1 μm (green and blue curves). The rms-roughness values are 0.59, 0.48, and 0.46 nm and the rms-slopes are 0.05, 0.20 and 0.19 for the red, green, and blue curves, respectively. The slope of the dashed line correspond to the Hurst exponent $H \approx 0.21$. Such small Hurst exponents are observed only on very smooth surfaces (small $h_{\rm rms}$) for reasons related to surface fragility (see Ref. 43). In Appendix B, we show the height probability distribution P_h and a topography image. The height distribution P_h is nearly Gaussian as expected for a randomly rough surface, but the theory presented above does not require the surface to be randomly rough.

IV. NUMERICAL RESULTS

For numerical calculations, it is convenient to write $qs = x$ so that (5) takes the form

$$F = E^* A_0 \frac{\pi}{s^4}\int_{q_0 s}^{q_1 s} dx\, x^3 C(x/s) J_1(x).$$

We introduce the shear stress $\tau = F/A_0$ and get

$$\frac{\tau}{E^*} = \frac{\pi}{s^4}\int_{q_0 s}^{q_1 s} dx\, x^3 C(x/s) J_1(x). \tag{6}$$

Since $J_1(x)$ oscillates as a function of x with a period of order 2π, it is necessary to use a uniform distribution of x-integration steps with step length $\Delta x \approx 0.1$ (or less) in order to evaluate the integral (6) numerically.

Figure 2 shows the shear stress τ divided by the effective Young's modulus E^* as a function of the logarithm of the displacement s. We have used the surface roughness power spectrum shown in Fig. 1. The red line is using the combined power spectra from the AFM data obtained on 1 and 10 μm scan lengths (green + red line in Fig. 1), while the green line is using only the 1 μm scan length data. Clearly, the shear stress is dominated by the large wavenumber part of $C(q)$, and the two calculations give nearly identical results. For surfaces with smaller fractal dimension (larger H), the long wavelength roughness becomes more important and the maximal stress

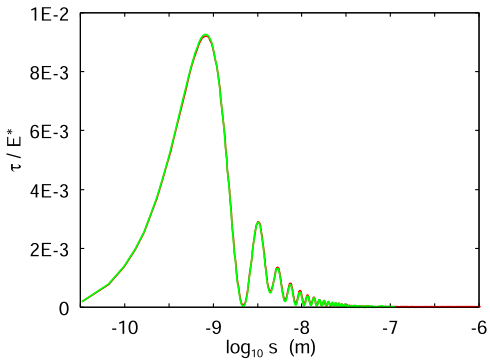

FIG. 2. The shear stress τ divided by the effective Young's modulus E^* as a function of the logarithm of the displacement s. The green and red lines are calculated for the surface roughness power spectrum given by the green line and the green + red line in Fig. 1.

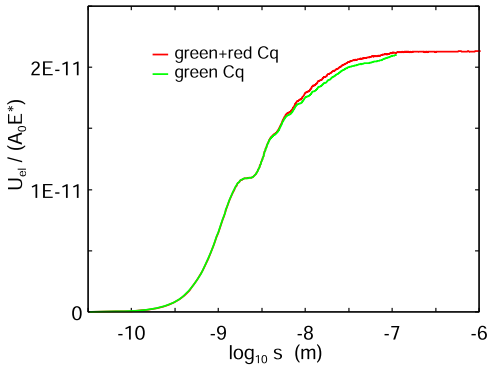

FIG. 3. The elastic energy per unit surface area divided by the effective Young's modulus E^* as a function of the logarithm of the displacement s. The green and red lines are calculated for the surface roughness power spectrum given by the green line and the green + red line in Fig. 1.

occurs at larger displacements. Thus, in these cases, U_{el} will reach its asymptotic value for larger displacements, which implies that the crack tip process zone will be longer (see Sec. V).

Another important quantity is the elastic energy stored at the interface[44] as a function of the displacement s. Figure 3 shows the elastic energy per unit surface area divided by the effective Young's modulus E^* as a function of the logarithm of the displacement s. Note again that using the power spectrum of the 1 μm scan length AFM data gives nearly the same result as the combined power spectrum from the 1 and 10 μm data.

V. INTERFACIAL CRACK PROPAGATION

If the shear stress τ given by (6) is very small (see below), then the bottom surface of the ice will displace uniformly due to the applied tangential force. However, this is not the case for the systems studied in Ref. 36 where instead an interfacial mode II (frictional) crack will propagate at the interface during onset of sliding (see Fig. 4).[45] Thus, the ice–substrate contact region will consist of two regions: one where slip has occurred and one where no slip has occurred. At the boundary line (crack tip) between these two regions occur a narrow strip (crack tip process zone) of width of order a few nm in the present case (but larger for surfaces with smaller fractal dimension) where the contact change from the commensurate-like no-slip state to the incommensurate-like slip state. The static or breakloose friction force is the determined by the force needed to move the crack tip, which depends on the crack propagation energy $G = U_{el}/A_0$.

The mode II crack propagation problem has been studied in many publications. If we assume that the kinetic frictional shear stress τ_k vanishes in the slip region (because of an ice premelted water film), then (see Appendix C and Ref. 46),

$$\sigma = \alpha\left(\frac{2EG}{h}\right)^{1/2},$$

where α is a dimensionless geometrical factor, which is of order unity if all length scales (height and length of the block, and height of the region over which the pressure σ is applied) are of similar

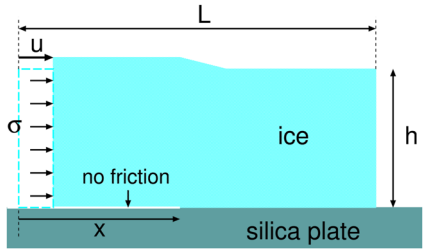

FIG. 4. A rectangular ice block in frozen contact with a silica substrate. On one side of the ice block, a stress or pressure σ is applied. The contact between the ice block and the substrate is broken by interfacial (type II) crack propagation. We assume that the ice–silica contact in the broken area $x < x_0$ exhibits zero friction (zero frictional shear stress).

magnitude. Thus, the effective frictional shear stress $\tau = F/A_0$, where $F = \sigma hw$ and $A_0 = wL$, is given by

$$\tau_s = \alpha\left(\frac{2EGh}{L^2}\right)^{1/2}. \tag{7}$$

In the present case, we have a cylinder shaped ice block with the height $h = 9$ mm and the diameter $L \approx 10$ mm so that $h/L \approx 1$; we expect α to be of order unity.

If the shear stress τ_{max} [given by (6)] is smaller than τ_s, then the slip at the interface at the onset of sliding will be (nearly) uniform, but if $\tau_s < \tau_{max}$, the onset of sliding will involve the interfacial crack propagation. If we write $G = \tau_{max}D$, where D is a distance of order the length of the crack-tip process zone, then in the present case, from Figs. 2 and 3, $D \approx 2.3$ nm. The condition $\tau_s = \tau_{max}$ gives

$$\tau_{max} = \alpha\left(\frac{2E\tau_{max}Dh}{L^2}\right)^{1/2}$$

or (with $\alpha = 1$)

$$\tau_{max} = \frac{2EDh}{L^2}. \tag{8}$$

This equation is equivalent to $\sigma = 2ED/L$. The stress σ acting on a block of length L gives a displacement u given by $\sigma = Eu/L$ or $u = L\sigma/E = 2D$. If the displacement u is smaller than the crack tip process zone (which is of order D), then the breakloose friction cannot be described by the crack propagation theory but is determined by (6). If $h \approx L \approx 1$ cm and $D \approx 5$ nm, then (8) gives for ice $\tau_{max} \approx 10^4$ Pa. In the present case, $\tau_{max} \approx 10^8$ Pa and interfacial crack propagation will occur.

Using ice Young's modulus $E = 9$ GPa and Poisson ratio $\nu = 0.3$, we get the effective modulus of ice $E^* = E/(1-\nu^2) \approx 10^{10}$ Pa and (from Fig. 3) $U_{el}/(E^*A_0) = 2.1 \times 10^{-11}$ m^{-1}, and we get $G = 0.21$ J/m^2. Using (7) with $L = 1$ cm and $\alpha = 1$, we get $\tau_s = 0.55$ MPa, which is close to the measured breakloose shear stress 0.75 MPa.

VI. DISCUSSION

In Ref. 36, the maximum (breakloose) shear stress $\tau_s = F_{max}/A_0$ was measured for ice blocks in frozen contact with a very smooth

silica surface with $h_{rms} \approx 0.45$ nm. Interfacial slip was observed for $-20\,^{\circ}\mathrm{C} < T < 0\,^{\circ}\mathrm{C}$ and the shear stress decreased linearly with $T_m - T$ as the temperature approached the melting temperature $T_m = 0\,^{\circ}\mathrm{C}$. For $T < -25\,^{\circ}\mathrm{C}$, cohesive fracture was observed. The breakloose shear stress for $T \approx -20\,^{\circ}\mathrm{C}$ was found to be $\tau_s \approx 0.75$ MPa, which we interpret as the shear stress when the premelted film is first formed and which may be of monolayer thickness. This shear stress can be compared to the theory prediction $\tau_s \approx 0.55$ MPa, assuming the surface roughness power spectrum shown in Fig. 1.

We note that the mode II (sliding) crack propagation energy found above, $G_{II} = G \approx 0.2$ J/m^2, is similar to the expected crack propagation energy for mode I (opening) crack propagation caused by the adhesive ice–countersurface interaction. For ice–ice adhesion, the (adiabatic) opening crack propagation energy $G_I = 2\gamma_{ice}$ is twice the surface energy per unit surface area of ice. The latter is[47] ≈0.1 J/m^2, so for the ice–ice interface, $G_I \approx 0.2$ J/m^2. We expect a similar interfacial binding energy for the ice–silica interface because the silica surface may be covered by a ~monolayer thick water film. The energy to propagate an opening crack may be larger than given above because of nonadiabatic effects. In addition, the normal stresses acting on the ice at the silica–ice interface are so high that some plastic deformations may occur in the ice at the sliding interface (see Appendix D).

Why does the breakloose shear stress decrease as the temperature T approaches the bulk melting temperature T_m? Here we propose the following explanation. Figure 5(a) shows ice in full adhesive contact with a hard substrate with sinus-like corrugation. If the ice is displaced laterally with a distance s equal to half the wavelength of the roughness profile, a positive pressure will result at the top of asperities and negative pressure in the valleys [see (b)]. As a result, water will flow in the premelted film from top of asperities to the bottom of the valleys. Since the premelted water film thickness must be approximately constant in time, ice must melt at the top of asperities and refreeze at the bottom of the valleys. Thus, ice is removed from the top of asperities and is added at the bottom of the wells. After some relaxation time t^*, the stress free state (c) is obtained. The relaxation time t^* depends on the temperature T and is shorter the closer the T is to the ice bulk melting temperature T_m because of the increased thickness of the premelted film and because of the increased mobility of the water molecules in the film as T increases.

If the time for the displacement s is much longer than t^*, the ice can nearly adiabatically adjust to the displacement and the breakloose friction force will nearly vanish. We believe this is the case close to the melting temperature T_m. However, as $T_m - T$ increases, the thickness of the premelted film decreases and the mobility of the water molecules decreases, and at some point, there is no time for the water to move from the top of asperities to the bottom of the valley resulting in the maximum in the breakloose friction force.

Experimentally, for very smooth surfaces (here a fused silica plate with the rms roughness ≈0.5 nm) for $-20\,^{\circ}\mathrm{C} < T < 0\,^{\circ}\mathrm{C}$, interfacial sliding is observed with the ice in complete contact with the substrate, with a friction force that decreases toward zero as the temperature approaches the ice melting temperature. We have proposed that this is due to changes in the thickness and molecule mobility of the water molecules in the premelted water film and to regelation. This reduces the elastic energy U_{el}/A_0 (the energy for type II crack propagation) with increasing temperature and finally results in a negligible breakloose force at the ice melting temperature.

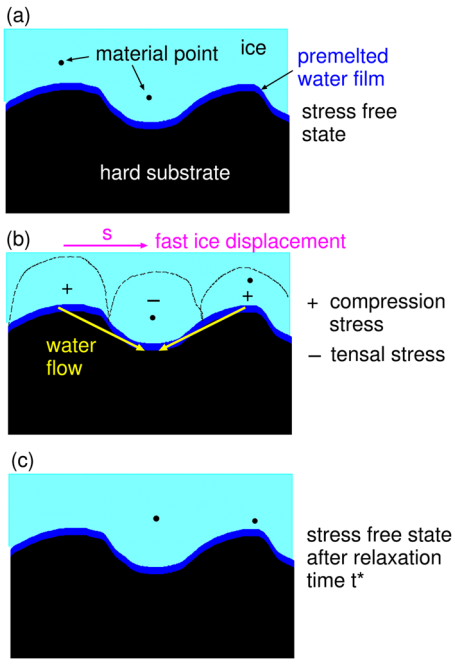

FIG. 5. (a) Ice in full adhesive contact with a hard substrate with a sinus-like corrugation. (b) The ice is displaced laterally with a distance s equal to half the wavelength of the roughness profile; it will result in positive pressure at the top of asperities and negative pressure in the valleys. As a result, water will flow in the premelted film from top of asperities to the bottom of the valleys. Since the premelted water film thickness must be approximately constant in time, ice is removed from the top of asperities and is added at the bottom of the wells. After some relaxation time t^*, the stress free state (c) is obtained. The relaxation time t^* depends on the temperature T and is shorter the closer the T is to the ice bulk melting temperature T_m because of the increased thickness of the premelted film and because of the increased mobility of the water molecules in the film as T increases.

A premelted film of water and regelation may occur also for $-25\,^{\circ}\mathrm{C} < T < -20\,^{\circ}\mathrm{C}$, but we have found that at $T \approx -20\,^{\circ}\mathrm{C}$, the elastic energy $G_{II} = U_{el}/A_0$ associated with the mode II (frictional) crack propagation becomes similar to the energy per unit area, G_I, to break the ice–substrate bonds in the normal direction as involved in type I crack propagation. This explains why the breakloose friction switches from interfacial sliding (type II crack propagation) to (type I) opening crack propagation at this temperature.

Here, it is interesting to note that an ice block on a silica surface with $h_{rms} \approx 0.8$ nm (when measured over a 2×2 μm^2 surface area) did (at $T = -10\,^{\circ}\mathrm{C}$) slide in adhesive contact, while this was not the case for any temperatures when $h_{rms} \approx 7.5$ nm where the contact broke by adhesive or cohesive failure.[36] When comparing these results to the theory, we need to take into account that because both the substrate and the ice surfaces have the same roughness, the effective h_{rms} is a factor of $\sqrt{2}$ bigger than h_{rms} of the substrate. This gives 1.1 and 10.6 nm for the two cases considered above.

The study presented above may be relevant for other types of systems. For example, viscoelastic solids have frequency dependent

modulus $E(\omega)$, where the low-frequency modulus $E_0 = E(0)$ may be much smaller than the high-frequency modulus $E_1 = E(\infty)$. In this case, when the surface roughness is so small that complete contact occur at the interface (because of adhesion) in both the static and the sliding state, a contribution to the breakloose friction force will come from the effect described above. That is, after long enough time of stationary contact, the substrate roughness induced elastic energy stored at the interface is determined by E_0, while at the onset of sliding, the viscoelastic solid behaves as a much stiffer material because of the high frequency perturbing deformations induced by the (short wavelength) substrate roughness (typical frequencies $\omega \approx qv$, where q is the wavenumber of a roughness component). However, in this case, the frictional shear stress is not negligible as assumed for ice (where a premelted water film is assumed to occur at the interface) and must be included in this study. In particular, a non-uniform shear stress would contribute to the energy stored at the interface and would change the definition of G_{II}. In addition, if the frictional stress in the sliding state is too big, elastic instabilities may occur (e.g., Schallamach waves), and the breakloose process will not involve the type of slip of the viscoelastic solid at the interface as assumed in the theory presented above.

Consider now a rubber block with a perfectly smooth surface in complete adhesive contact with a rigid substrate with at most nanoscale surface roughness. We assume that the temperature is so high and contact time is so long that the rubber effectively is in the rubbery state with the elastic modulus E_0. Next, the temperature is lowered so that the rubber reach its glassy state where the elastic modulus is E_1. The deformation field induced in the rubber is "frozen-in" when the temperature is lowered to the glassy state. Thus, the force to displace the rubber block will again be given by the theory above with the elastic modulus given by the rubber modulus in the glassy state, which typically is similar to that of ice. Of course, if the roughness amplitude is larger than ~1 nm, the contact may no longer be complete in the displaced state, in which case the breakloose force would instead be determined mainly by the change in the interfacial binding energy.

VII. ICE ADHESION TO WINDOW GLASS

People living in countries with cold winters know that it is not easy to remove ice formed on automobile windshields.[49] Window glass, e.g., windshields, are produced from float glass. Float glass is a sheet of glass made by floating molten glass on a bed of molten metal, typically tin. This results in very smooth surfaces, which in ideal cases would have surface roughness resulting only from frozen capillary waves. Frozen capillary waves have the surface roughness power spectrum (see, e.g., Refs. 51 and 52)

$$C(q) = \frac{1}{(2\pi)^2}\frac{k_b T^*}{\rho g + \gamma q^2}. \tag{9}$$

Here, we have assumed that when reaching the temperature T^*, the diffusive movement of the atoms in the glass becomes so slow that the capillary waves that exist at this temperature are frozen. Note that the gravity term ρg becomes important only for very small wavenumber roughness, namely, for $q < (\rho g/\gamma)^{1/2} \approx 300\ \mathrm{m}^{-1}$, and the gravity term can be neglected in most cases giving $C(q) \sim q^{-2}$, which corresponds to a self-affine fractal surface with the Hurst exponent $H = 0$ (and fractal dimension $D_f = 3$). For such surfaces, the rms slope is determined mainly by the shortest (nanometer) wavelength roughness. Real glass surfaces have larger roughness than predicted by (9) because of effects such as mechanical vibrations during cooling from the melted state or scratches from mechanical interactions or weathering.[53]

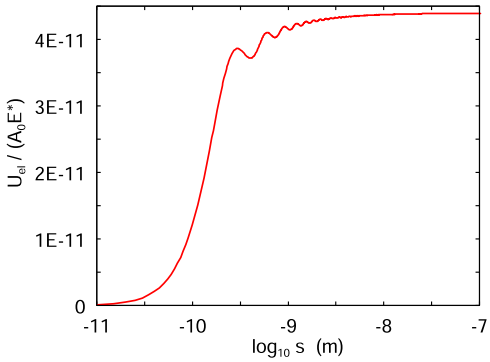

FIG. 6. The elastic energy per unit surface area divided by the effective Young's modulus E^* as a function of the logarithm of the displacement s. For the surface roughness, the power spectrum is given by (9).

Using the power spectrum given by (9) with $T^* = 600$ K, $\gamma = 0.3\ \mathrm{J/m^2}$, and $\rho = 2200\ \mathrm{kg/m^2}$ and including the roughness wavenumber range $q_0 < q < q_1$ with $q_0 = 300\ \mathrm{m}^{-1}$ and $q_1 = 2 \times 10^{10}\ \mathrm{m}^{-1}$ give the rms roughness amplitude $h_{\mathrm{rms}} = 0.27$ nm and the rms slope $\xi = 0.95$. In Fig. 6, we show the elastic energy per unit surface area (4) divided by the effective Young's modulus E^* as a function of the logarithm of the displacement s obtained for the surface roughness power spectrum given by (9). The asymptotic value for $G = U_{el}/A_0$ for large displacement (here only $s \approx 10$ nm) is given by (A2), $G \approx E^*\xi^2 q_1$. Because of the large rms slope for frozen capillary waves, the elastic energy per unit surface area produced when the ice displaced away laterally from its original position is $G \approx 0.45\ \mathrm{J/m^2}$. This is even larger than found above for the silica surface (see Fig. 1) because the surface roughness of the glass surface with capillary waves has a larger fractal dimension. Thus, we expect cohesive failure rather than adhesive failure at the ice–glass interface. This explains why it is hard to remove ice from the windshields of cars even for temperatures (say $T = -5\,^\circ\mathrm{C}$) where one expects a very thin water film of premelted ice.

VIII. SUMMARY AND CONCLUSIONS

To summarize, we have proposed a new mechanism for the ice breakloose friction force on very smooth substrate surfaces. The ice in the initial state is assumed to adhere fully in a stress free state on the substrate, and the breakloose force is associated with the roughness induced elastic energy stored at the interface as the ice is displaced laterally relative to the substrate. The temperature dependency of the breakloose friction force is attributed to regelation resulting from premelting.

Experimentally (see Ref. 36), for ice frozen on top of a silica surface with the rms roughness ≈0.5 nm with decreasing temperature, we observe the following three different breakloose scenarios:

(a) *Sliding breakloose*: the ice is sliding in full (adhesive) contact with the substrate.
(b) *Adhesive breakloose*: ice–substrate bonds are broken, resulting in a transition to partial contact but with no ice left on the countersurface.
(c) *Cohesive breakloose*: the shear plane occur inside the ice. In this case, ice is left on the countersurface.

It is clear that if the roughness is big enough, the breakloose due to a tangential force will always occur by process (c), and during slip, the hard substrate asperities will plow the ice surface, resulting in ice wear and a contribution to the sliding friction from the plowing.

Experimentally, for very smooth surfaces (here a fused silica window with the rms roughness ≈0.5 nm), all three processes (a)–(c) occur depending on the temperature. For $-20\,^{\circ}\mathrm{C} < T < 0\,^{\circ}\mathrm{C}$, process (a) occurs with a breakloose friction force, which decreases toward zero as the temperature approaches the ice melting temperature. We have proposed that this is due to changes in the thickness and the mobility of the water molecules in the premelted water film and to regelation. This reduces the elastic energy U_{el}/A_0 (the energy for type II crack propagation) with increasing temperature and finally results in a negligible breakloose force at the ice melting temperature.

A premelted film of water and regelation may occur also for $-25\,^{\circ}\mathrm{C} < T < -20\,^{\circ}\mathrm{C}$, but we have found that at $T \approx -20\,^{\circ}\mathrm{C}$, the elastic energy $G_{\mathrm{II}} = U_{\mathrm{el}}/A_0$ associated with the mode II (frictional) crack propagation becomes similar to the energy per unit area, G_{I}, to break the ice–substrate bonds in the normal direction as involved in type I crack propagation. This explains why the nature of the breakloose friction switches from process (a) (type II crack propagation) to (b) (type I crack propagation) at this temperature.

ACKNOWLEDGMENTS

E.C.T. acknowledges support from the Swedish Research Council (VR). We thank Trinh Nguyen and Matthew Fielden for their help when performing the AFM topography measurements.

AUTHOR DECLARATIONS

Conflict of Interest

The authors have no conflicts to disclose.

Author Contributions

B. N. J. Persson: Conceptualization (equal); Data curation (equal); Formal analysis (equal); Funding acquisition (equal); Investigation (equal); Methodology (equal); Project administration (equal); Resources (equal); Software (equal); Supervision (equal); Validation (equal); Visualization (equal); Writing – original draft (equal); Writing – review & editing (equal). **E. C. Tyrode**: Conceptualization (equal); Data curation (equal); Formal analysis (equal); Funding acquisition (equal); Investigation (equal); Methodology (equal); Project administration (equal); Resources (equal); Software (equal); Supervision (equal); Validation (equal); Visualization (equal); Writing – original draft (equal); Writing – review & editing (equal).

DATA AVAILABILITY

The data that support the findings of this study are available from the corresponding author upon reasonable request.

APPENDIX A: CRACK ENERGY G FOR SELF AFFINE FRACTAL ROUGHNESS

For $q_1 s \gg 1$, we can neglect the $J_0(qs)$ term in (4) since the amplitude of $J_0(x)$ for large x varies as $x^{-1/2}$. Thus, for large displacement s, we get

$$G = \frac{U_{\mathrm{el}}}{A_0} = \pi E^* \int_{q_0}^{q_1} dq\; q^2 C(q).$$

Assume that for $q_0 < q < q_1$,

$$C(q) = C_0 \left(\frac{q}{q_0}\right)^{-2(1+H)}$$

and $C(q) = 0$ for $q > q_1$ and $q < q_0$. We get

$$G = \frac{E^* \xi^2}{2} \frac{\int_{q_0}^{q_1} dq\; q^2 (q/q_0)^{-2(1+H)}}{\int_{q_0}^{q_1} dq\; q^3 (q/q_0)^{-2(1+H)}}.$$

Writing $q = q_0 x$, we get

$$G = \frac{E^* \xi^2}{2q_0} \frac{\int_1^{q_1/q_0} dx\; x^{-2H}}{\int_1^{q_1/q_0} dx\; x^{1-2H}}$$

or

$$G = \frac{E^* \xi^2}{q_0} \frac{1-H}{1-2H} \frac{1-(q_1/q_0)^{1-2H}}{1-(q_1/q_0)^{2-2H}}. \tag{A1}$$

For $H = 0$, this gives

$$G = \frac{E^* \xi^2}{q_0} \frac{1-(q_1/q_0)}{1-(q_1/q_0)^2} \approx \frac{E^* \xi^2}{q_1}, \tag{A2}$$

where we have used that $q_1/q_0 \gg 1$ in all cases of interest. As $H \to 1$, we get

$$G \approx \frac{E^* \xi^2}{2q_0} \frac{1}{\ln(q_1/q_0)}. \tag{A3}$$

Using that the rms roughness amplitude h_{rms} is obtained as

$$h_{\mathrm{rms}}^2 = \int d^2 q\; C(q),$$

and we get

$$\frac{\xi^2}{q_0^2 h_{\mathrm{rms}}^2} = \frac{H}{H-1} \frac{1-(q_1/q_0)^{2(1-H)}}{1-(q_1/q_0)^{-2H}}.$$

APPENDIX B: SURFACE ROUGHNESS TOPOGRAPHY

Figure 7 shows an AFM topography map from a 1 μm × 1 μm surface region of the polished silica surface used in calculating the

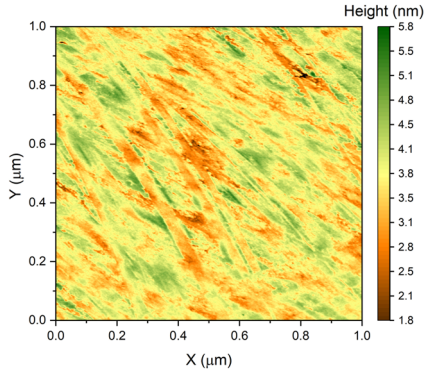

FIG. 7. The surface height of the silica substrate as obtained from AFM topography measurements (1024 × 1024 data points) over a square area with the side 1 μm. The topography was used when calculating the green $C(q)$ curve in Fig. 1.

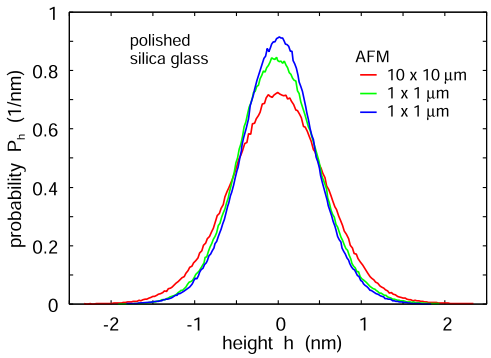

FIG. 8. The surface height probability distribution P_h of the silica substrate as obtained from AFM topography measurements (1024 × 1024 data points) over square areas with the side 10 μm (red curve) and 1 μm (green and blue curves). P_h is nearly Gaussian as expected for a randomly rough surface.

green line in Fig. 1. Note the polishing tracks that can be observed also on other surface area (not shown).

Figure 8 shows the surface height probability distribution P_h over square areas with the side 10 μm (red curve) and 1 μm (green and blue curves). Note that P_h is nearly Gaussian as expected for a randomly rough surface.

For another study of the surface roughness of polished fused quartz, see Ref. 48.

APPENDIX C: BREAKLOOSE FORCE

We assume that the onset of sliding occur by interfacial mode II (frictional) crack propagation at the interface. Thus, the ice–substrate contact region will consist of two regions: one where slip has occurs and one where no slip has occurred. At the boundary line (crack tip) between these two regions occurs a narrow strip (crack tip process zone, of width a few nm in the present applications) where the contact changes from the commensurate-like no-slip state to the incommensurate-like slip state. The static or breakloose friction force is the force needed to move the crack tip, which depend on the crack propagation energy $G = U_{el}/A_0$.

The mode II interfacial crack propagation problem has been studied in many publications, but here we give for the readers convenience a simple summary of the basic theory for the simplest case where the kinetic frictional stress τ_k in the slip region can be neglected (for a treatment including τ_k, see Ref. 46), and we neglect edge effects. Consider a rectangular ice block in frozen contact with a silica substrate (see Fig. 4). On the one side of the ice block, a pressure or stress σ is applied. The contact between the ice block and the substrate is broken by interfacial crack propagation. We assume that the ice–silica contact in the broken area $x < x_0$ exhibits zero friction (zero frictional shear stress). To increase the length of the frictional crack (mode II crack) by Δx requires an energy $Gw\Delta x$, where w is the width of the block in the y-direction and where $G = U_{el}/A_0$ is given in Fig. 3. This energy is supplied by the external stress σ. Thus, if the crack length increases with Δx, the surface where the pressure acts will move with the distance u determined by $\sigma = Eu/\Delta x$, where $u/\Delta x$ is the strain in a Δx wide slab of material on the cracked side of the ice block. Thus, the external work is

$$U_\sigma = \sigma h w u = \frac{\sigma^2}{E} h w \Delta x.$$

This external work is partly used at the interface to move the ice over the roughness barrier, $Gw\Delta x$, and partly stored as bulk elastic energy in the added segment Δ x of compressed solid,

$$U_{el} = \frac{1}{2}\sigma\epsilon h w \Delta x = \frac{1}{2}\frac{\sigma^2}{E} h w \Delta x.$$

Using $U_\sigma = U_{el} + Gw\Delta x$ gives

$$\frac{1}{2}\frac{\sigma^2}{E} h w \Delta x = Gw\Delta x$$

or

$$\sigma = \left(\frac{2EG}{h}\right)^{1/2}.$$

Thus, the effective frictional shear stress $\tau = F/A_0$, where $F = \sigma h w$ and $A_0 = wL$, is given by

$$\tau = \left(\frac{2EGh}{L^2}\right)^{1/2}.$$

In the present case, we have a cylinder shaped ice block. For this case, we denote the maximum effective shear stress by

$$\tau_s = \alpha\left(\frac{2EGh}{L^2}\right)^{1/2}, \tag{C1}$$

where α is a dimensionless geometrical factor that depends on the ratio h/L (where $h \approx 9$ mm is the height of the ice cylinder and $L \approx 10$ mm the diameter of the ice cylinder), and since $h/L \approx 1$, we expect α to be of order unity.

APPENDIX D: RMS NORMAL STRESS FLUCTUATIONS

Here, we derive the normal rms stress at the interface. We have[39]

$$\langle\sigma^2\rangle = \frac{(2\pi)^2}{A_0}\int d^2q\ \langle\sigma(\mathbf{q})\sigma(-\mathbf{q})\rangle.$$

Using that[40]

$$\sigma(\mathbf{q}) = \frac{1}{2}E^* q u(\mathbf{q}),$$

we get

$$\langle\sigma^2\rangle = \frac{(2\pi)^2}{A_0}\left(\frac{E^*}{2}\right)^2\int d^2q\ q^2\langle u(\mathbf{q})u(-\mathbf{q})\rangle.$$

Using (1) and (3), this gives

$$\langle\sigma^2\rangle = \pi\left(E^*\right)^2\int dq\ q^3C(q)[1-J_0(qs)]. \tag{D1}$$

We will denote $\langle\sigma^2\rangle = \sigma_{\rm rms}^2$. Note that for large displacement s,

$$\langle\sigma^2\rangle \approx \pi\left(E^*\right)^2\int dq\ q^3C(q) = \frac{1}{2}\left(\xi E^*\right)^2 \tag{D2}$$

or $\sigma_{\rm rms}/E^* \approx \xi/\sqrt{2}$.

Figure 9 shows the average shear stress τ (red line) and the average normal stress $\sigma_{\rm rms}$ (blue) divided by the effective Young's modulus E^* as a function of the logarithm of the displacement s for the surface roughness power spectrum shown by the green + red line in Fig. 1. Note that when the shear stress is maximal, the rms-average normal stress is about 15 times bigger than the shear stress, and that $\sigma_{\rm rms} \to \xi E^*/\sqrt{2}$ as the displacement $s \to \infty$, while the tangential stress $\tau \to 0$ as $s \to \infty$. The stress needed to plastically deform ice depends on the ice temperature and the deformation rate and is typically rather low under most practical conditions of order 10 MPa for $T = -10\,^\circ$C and the strain rates 1 s^{-1}. At very short (nanometer) length scale, which is relevant for the applications in this paper where the crack-tip process zone is of order a few nm, the plastic yield stress may be much higher. Short wavelength roughness generates very high deformation rates even at low sliding speeds, and under this condition, thermal activation is strongly reduced, and since dislocations and other imperfections usually involved in plastic deformation of ice may be less important at the nanoscale, the plastic yield stress may be close to its ideal value αE, where $\alpha \approx 0.1$ (see Ref. 54). We conclude that nanoscale roughness may result in plastic deformation if the rms slope ξ is larger than ~0.1, which is close to the rms slope we found on the polished fused silica plate. However, molecular dynamics studies of ice sliding on a corrugated substrate are needed to better understand the role of plastic deformations.

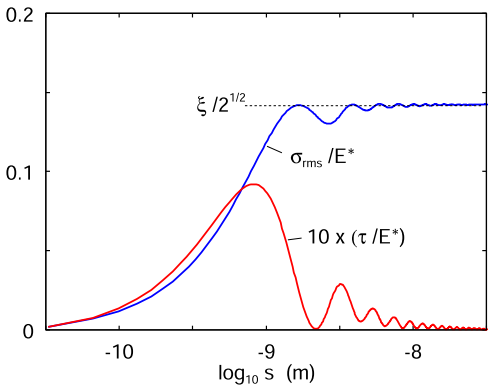

FIG. 9. The average shear stress τ (red line) and the average normal stress $\sigma_{\rm rms}$ (blue) divided by the effective Young's modulus E^* as a function of the logarithm of the displacement s. The surface roughness power spectrum is shown by the green + red line in Fig. 1.

REFERENCES

[1] R. Rosenberg, "Why is ice slippery?," Phys. Today **58**(12), 50 (2005).
[2] A.-M. Kietzig, S. G. Hatzikiriakos, and P. Englezos, "Physics of ice friction," J. Appl. Phys. **107**, 081101 (2010).
[3] J. F. Nye, "Glacier sliding without cavitation in a linear viscous approximation," Proc. R. Soc. A **315**, 381 (1970).
[4] B. N. J. Persson, "Ice friction: Glacier sliding on hard randomly rough bed surface," J. Chem. Phys. **149**, 234701 (2018).
[5] L. Bäurle, T. U. Kaempfer, D. Szabó, and N. D. Spencer, "Sliding friction of polyethylene on snow and ice: Contact area and modeling," Cold Reg. Sci. Technol. **47**, 276 (2007).
[6] R. W. Liefferink, F. C. Hsia, B. Weber, and D. Bonn, "Friction on ice: How temperature, pressure, and speed control the slipperiness of ice," Phys. Rev. X **11**, 011025 (2021).
[7] L. Canale, J. Comtet, A. Nigues, C. Cohen, C. Clanet, A. Siria, and L. Bocquet, "Nanorheology of interfacial water during ice gliding," Phys. Rev. X **9**, 041025 (2019).
[8] M. E. H. van Dongen and D. M. J. Smeulders, "Ice speed skating: Onset of lubrication by frictional heating," Europhys. Lett. **134**, 34005 (2021).
[9] A. D. Roberts, "Rubber-ice adhesion and friction," J. Adhes. **13**, 77 (1981).
[10] A. D. Roberts and J. C. Richardson, "Interface study of rubber-ice friction," Wear **67**, 55 (1981).
[11] D. D. Higgins, B. A. Marmo, C. E. Jeffree, V. Koutsos, and J. R. Blackford, "Morphology of ice wear from rubber-ice friction tests and its dependence on temperature and sliding velocity," Wear **265**, 634 (2008).
[12] O. Lahayne, B. Pichler, R. Reihsner, J. Eberhardsteiner, J. Suh, D. Kim, S. Nam, H. Paek, B. Lorenz, and B. N. J. Persson, "Rubber friction on ice: Experiments and modeling," Tribol. Lett. **62**, 17 (2016).
[13] N. Orndorf, S. Singla, and A. Dhinojwala, "Transition in the acid-base component of surface free energy of ice upon the premelting of its second molecular bilayer," J. Phys. Chem. C **124**, 19588 (2020).
[14] Ł. Baran, P. Llombart, W. Rżysko, and L. G. MacDowell, "Ice friction at the nanoscale," Proc. Natl. Acad. Sci. U. S. A. **119**(49), e2209545119 (2022).
[15] A. J. Tuononen, A. Kriston, and B. Persson, "Multiscale physics of rubber-ice friction," J. Chem. Phys. **145**, 114703 (2016).
[16] C. Klapproth, T. M. Kessel, K. Wiese, and B. Wies, "An advanced viscous model for rubber-ice-friction," Tribol. Int. **99**, 169 (2016).
[17] F. E. Kennedy, E. M. Schulson, and D. E. Jones, "The friction of ice on ice at low sliding velocities," Philos. Mag. A **80**, 1093 (2000).
[18] B. N. J. Persson, "Ice friction: Role of non-uniform frictional heating and ice premelting," Chem. Phys. **143**, 224701 (2015).
[19] S. Hemette, J. Cayer-Barrioz, and D. Mazuyer, "Thermal effects versus viscoelasticity in ice-rubber friction mechanisms," Tribol. Int. **162**, 107129 (2021).
[20] F. P. Bowden, "Friction on snow and ice," Proc. R. Soc. London, Ser. A **217**, 462 (1953).
[21] A. Almqvist, B. Pellegrini, N. Lintzén, N. Emami, H.-C. Holmberg, and R. Larsson, "A scientific perspective on reducing ski-snow friction to improve performance in Olympic cross-country skiing, the biathlon and Nordic combined," Front. Sports Act. Living **4**, 844883 (2022).

[22]K. Kalliorinne, B. N. J. Persson, J. Sandberg, G. Hindér, R. Larsson, H.-C. Holmberg, and A. Almqvist, "Snow contact characterisation of cross-country skis: A macro-scale study of the apparent contact," Lubricants **11**, 225 (2023).
[23]M. Faraday, "On regelation, and on the conservation of force," Philos. Mag. **17**, 162 (1859).
[24]J. W. M. Frenken and J. F. Van Der Veen, "Observation of surface melting," Phys. Rev. Lett. **54**, 134 (1985).
[25]B. Slater and A. Michaelides, "Surface premelting of water ice," Nat. Rev. Chem. **3**, 172 (2019).
[26]R. Lipowski, "Critical surface phenomena at first-order bulk transitions," Phys. Rev. Lett. **49**, 1575 (1982).
[27]U. Tartaglino, T. Zykova-Timan, F. Ercolessi, and E. Tosatti, "Melting and nonmelting of solid surfaces and nanosystems," Phys. Rep. **411**, 291 (2005).
[28]D. T. Limmer "Closer look at the surface of ice," Proc. Natl. Acad. Sci. U. S. A. **113**, 12347 (2016).
[29]Y. Qiu and V. Molinero, "Why is it so difficult to identify the onset of ice premelting?," J. Phys. Chem. Lett. **9**, 5179 (2018).
[30]Y. Li and G. A. Somorjai, "Surface premelting of ice," J. Phys. Chem. C **111**, 9631 (2007).
[31]E. S. Thomson, H. Hansen-Goos, J. S. Wettlaufer, and L. A. Wilen, "Grain boundary melting in ice," J. Chem. Phys. **138**, 124707 (2013).
[32]M. Torabi Rad, G. Boussinot, and M. Apel, "Dynamics of grain boundary premelting," Sci. Rep. **10**, 21074 (2020).
[33]M. Demmenie, P. Kolpakov, Y. Nagata, S. Woutersen, and D. Bonn, "Scratch-healing behavior of ice by local sublimation and condensation," J. Phys. Chem. C **126**, 2179 (2022).
[34]J. Thomson, "On recent theories and experiments regarding ice at or near its melting-point," Proc. R. Soc. London **10**, 151 (1859).
[35]F. P. Bowden and T. P. Hughes, "The mechanism of sliding on ice and snow," Proc. R. Soc. London, Ser. A **172**, 280 (1939).
[36]J. F. D. Liljeblad, I. Furó, and E. C. Tyrode, "The premolten layer of ice next to a hydrophilic solid surface: Correlating adhesion with molecular properties," Phys. Chem. Chem. Phys. **19**, 305 (2017).
[37]H. H. G. Jellinek, "Ice adhesion," Can. J. Phys. **40**, 1294 (1962).
[38]S. Yamaguchi, Y. Suzuki, and T. Otosu, "Perspective on sum frequency generation spectroscopy of ice surfaces and interfaces," Chem. Phys. **522**, 199 (2019).
[39]B. N. J. Persson, "On the elastic energy and stress correlation in the contact between elastic solids with randomly rough surfaces," J. Phys.: Condens. Matter **20**, 312001 (2008).
[40]B. N. J. Persson, "Theory of rubber friction and contact mechanics," J. Chem. Phys. **115**, 3840 (2001).
[41]P. R. Nayak, "Random process model of rough surfaces," ASME J. Lubr. Technol. **93**, 398 (1971).
[42]B. N. J. Persson, O. Albohr, U. Tartaglino, A. I. Volokitin, and E. Tosatti, "On the nature of surface roughness with application to contact mechanics, sealing, rubber friction and adhesion," J. Phys.: Condens. Matter **17**, R1 (2004).
[43]B. N. J. Persson, "On the fractal dimension of rough surfaces," Tribol. Lett. **54**, 99 (2014).
[44]B. N. J. Persson, "Adhesion between an elastic body and a randomly rough hard surface," Eur. Phys. J. E **8**, 385 (2002).
[45]T. L. Anderson, *Fracture Mechanics, Fundamentals and Applications*, 3rd ed. (CRC Press, 2004).
[46]B. Lorenz and B. N. J. Persson, "On the origin of why static or breakloose friction is larger than kinetic friction, and how to reduce it: The role of aging, elasticity and sequential interfacial slip," J. Phys.: Condens. Matter **24**, 225008 (2012).
[47]L. B. Boinovich and A. M. Emelyanenko, "Experimental determination of the surface energy of polycrystalline ice," Dokl. Phys. Chem. **459**, 198 (2014).
[48]N. I. Chkhalo, S. A. Churin, A. E. Pestov, N. N. Salashchenko, Y. A. Vainer, and M. V. Zorina, "Roughness measurement and ion-beam polishing of super-smooth optical surfaces of fused quartz and optical ceramics," Opt. Express **22**, 20094 (2014).
[49]Y. Zhang, Y. Zhang, R. Guo, and B. Cui, "Method for testing shear and tensile strengths of freshwater/seawater ice," Water **14**, 1363 (2022).
[50]Y. Zhao, Y. Wu, L. Bao, F. Zhou, and W. Liu, "A new mechanism of the interfacial water film dominating low ice friction," J. Chem. Phys. **157**, 234703 (2022).
[51]B. N. J. Persson "Influence of frozen capillary waves on contact mechanics," Wear **264**, 746 (2008).
[52]B. N. J. Persson, "Contact mechanics for randomly rough surfaces," Surf. Sci. Rep. **61**, 201 (2006).
[53]N. Miyashita, A. E. Yakini, W. Pyckhout-Hintzen, and B. N. J. Persson, "Sliding friction on ice," J. Chem. Phys. **158**, 174702 (2023).
[54]B. N. J. Persson, "Surface roughness induced stress concentration," Tribol. Lett. **71**, 66 (2023); arXiv:2304.02159.